International Journal Of Engineering Research And Development
e- ISSN: 2278-067X, p-ISSN: 2278-800X, www.ijerd.com
Volume 19, Issue 1 (Jan.-Feb. 2023), PP. 17-37

Computational Fluid Dynamic Analysis of Ahmed Body in Martian Environment

Syed Muhammad Arafat[1, 2], Muhammad Waqas Aslam[1,] Sajawal Gul Niazi[3], Ghulam Moeen Uddin[1], Muhammad Umar Malkana[4], Abdul Rehman[5], Muhammad Zeeshan Nawaz[1],SyedWasim Hassan Zubair[1],Abdul Raheem[2],Raees Ahmad[2], Muhammad Athar Mahmood[1], Muhammad Arif[1],Muhammad Talha Saeed[1], Muhammad Talha Nawazish[1],Umer Farooq[1], Abe Zeid[6*]

1 Department of Mechanical Engineering, University of Engineering & Technology, Lahore 54890, Pakistan
2 Department of Mechanical Engineering, Faculty of Engineering & Technology, The University of Lahore, Lahore 54000, Pakistan
3 School of Mechanical and Electrical Engineering, University of Electronic Science and Technology of China,Chengdu 611731, China
4 Mechanical Engineering Department, University of Gujrat Hafiz Hayat Campus
5 Punjab Tianjin University of Technology, Lahore, Pakistan
6 Department of Mechanical & Industrial Engineering, NortheasternUniversity, Boston, MA, USA
**Corresponding author: Abe Zeid, Department of Mechanical & Industrial Engineering, Northeastern University, 334 Snell Engineering Center, 360 Huntington Avenue, Boston, MA 02115, USA.*

Abstract
This research work presents the computational aerodynamic study of Ahmed body situated in Martian environment in comparison with Earth's environment. The hybrid RANS-LES model with the dynamic Smagorinsky-Lilly method is used to capture flow characteristics of the wake region of Ahmed body. A comprehensive mesh independence study is conducted to obtain the results, which are approximately unaffected by mesh resolution. The impact of three critical variables i.e., slant angle, stream velocity and temperature is analyzed on flow behavior. It is observed that the difference in Martian and Earth environment have considerable effect on coefficient of drag experienced by the Ahmed body. It is also found that the slant angle plays a vital role in aerodynamic performance of Ahmed body. A noticeable difference in coefficient of drag is observed by changing the temperature for Mars environment. Human beings have wasted a lot of Earth's resources in past and this issue can be avoided by informed design decisions in Mars colonization process. Surface vehicles are resource consuming devices and the power consumption of a surface vehicle is directly linked with the study of aerodynamic flow. Therefore, it is logical to give attention to this subject matter.
Keywords: *Ahmed Body, CFD in Martian environment, vehicle aerodynamics, Fluid flow analysis of Ahmed body, Mars*

Date of Submission: 22-02-2023 Date of Acceptance: 05-03-2023

List of Nomenclature & Abbreviations:		*Y/L*	Distance in Y direction divided by length of Ahmed body
RANS	Reynolds-averaged Navier–Stokes	*u/U*□	X-velocity component divided by the far field velocity
LES	Large Eddy Simulation	C_p	Coefficient of pressure
C_D	Coefficient of drag	E288	Earth case at 288K temperature
C_L	Coefficient of lift	M210	Mars case at 210K temperature
T	Temperature	E298	Earth case at 298K temperature
CFD	Computational fluid dynamics	M298	Mars case at 298K temperature
L	Length of Ahmed body	SM	Smagorinsky-Lily model
R	Shoulder Radius	DSM	Dynamic Smagorinsky-Lily model
n	Number of elements	Greek Symbols:	
DSM	Dynamic Smagorinsky-Lily	φ	Slant Angle

	model		
X/L	Distance in X direction divided by length of Ahmed body	Ω	Velocity Vortices

I. Introduction

The focus on studies related to Mars that include the understanding of Martianenvironment and application of different equipment, devices and living organism behavior (history and future) are growing in past few decades. The possibility of life on Mars either in recent times or in distant past or even at present is an important and critical topic for researchers[1-3]. The study related to the possibility of photosynthetic potential zone in comparison to Earth was conducted to understand the possibility of colonization of photosynthetic organisms [4].Vera et. al., demonstrated that the Antarctic lichen can adapt to Martian environment in just thirty-four days[5].Different studies regarding human missions on Mars were also conducted in recent decades.

Possibility of human existence on Mars seemscloser as discussed in literature available by NASA [6, 7]. Attempts to find out the clear possibility of human landing on Mars and plans to colonize Mars have been made by different space agencies and private entities.The problems which are currently being addressed for Mars human colonization include every aspect of scientific and social science; for example, what type of initial equipment can be used on test sites, or nuclear power generation consideration etc., [8, 9].

A typical concern in Mars colonization isthat we should not repeat mistakes which we have made on Earth while colonizing it [10]. Therefore, a large number of machines or devices that need to be present at Mars as human colonize it, must be efficient and less harmful to Martianenvironment. Researchers are utilizing the data available from unmanned missions on Mars and other sources to recreate Martian environment in labs or especially in computer simulations to study and understand the behavior of machines and equipment. The heat transfer study along with the behavior of flowing fluid was conducted with the results of heat transfer in horizontal and vertical enclosures on Martian environment [11]. Similarly, different procedure for power generation in the Martian environment with their possibilities and efficiencies are given by recent studies [12-15].The ability to transport goods, equipment and humans from one site to another on Mars is of great importance. Different Mars rovers need to cover large distance to collect data as in case of Jet Propulsion Laboratory (JPL) curiosity. Similarly, there might be a possibility that goods and especially humans may requirean acceptable[16]and fast transportation system which includes all kind of vehicles to travel from one colony site to the next colony site.Therefore, different types of vehicle for different types of work need to be investigated.

Several examples exist in literature in which researchers are interested to work on different vehicle forms for Martian environment.To exit Mars surface with humans, Mars ascent vehicle design was proposed and research work on different aspects of Mars ascent vehicle was conductedby the researchers[17-19]. Cargo vehicles for human missions on Mars were also found in recent studies [20]. Crewed vehicles and other mobility vehicles was acknowledged by a study sponsored by NASA [21, 22]. Surface vehicles were discussed with respect to their terrain requirements, size and the power consumption needed etc. Similarly, previous research indicates that some key resources like minerals and water requiredfor a sustainable human society on Mars may be obtained far away from the residence area [23]. Surface vehicles especially the vehicles working as human transporters on Mars are currently in focus and carryexcessive interest.

The power consumption of surface vehicle is directly linked with the study of aerodynamic flow. It is important to have a comparative study on both Martian and Earth environments. The Ahmed body is the simplest form of vehicle shape representing passenger cars on Earth[24-26]. Therefore, to understand the basics of vehicle aerodynamics working as human transporters on Martian surface, Ahmed body is an appropriate choice.

Experimental aerodynamic study is conducted in wind tunnel which can represent the full-scale experimental testing of a car-like body. Virtual wind tunnel can be used for the numerical basedaerodynamic studies of different vehicles shapes[25, 27]. To study the flow characteristics and aerodynamics of vehicles, efficient numerical models are required; Reynolds Averaged Navier-Stokes (RANS) is one of those models extensively usedby industry today. RANS model has been found very successful in analyzing the flow characteristics around many parts of the vehicle; however, this model fails in the prediction of unsteadiness in the wake regions[28]. Another model termed as Large Eddy Simulations (LES) model is found useful for predicting the unsteadiness which is not resolved in RANS model. However, the choice between RANS and LES is also dependent on the computational power of the system along with the required accuracy[29].To predict the flow characteristics in highly separated regions, Spalart et al [30] proposed a hybrid approach- a combination of RANS and Large Eddy Simulations (LES) method.Hybrid approach, compared to simple LES model, has been found to have higher accuracy which is maintained even at very high Reynolds number flows[31].

Slant angle (φ) in the aerodynamic study of vehicle has also been found influential in Earth environment.Tunay, T., et al., varied the slant angle from 25° to 35° with a step of 5° and studied their effects on

wake flow characteristics on the downstream side of the Ahmed body as flow separation downstream of the Ahmed body contributes to most of its drag [32]. Similarly, the effect of slant angle(φ) of the upper rear section of Ahmed bodyon flow characteristics has been investigated and presented in literature [26, 33].

Along with the slant angle, flow characteristics and thus the coefficient of drag (C_D) are also affected by the velocity of flow stream[34].Various studies have also been conducted in this regard to investigate the effect of velocity on coefficient of drag e.g. Bello-Millán, F., et al., found that $C_D$decreases slightly with the increase in Reynolds number[35]. Mohammadikalakoo, B., et al.[26] performed the numerical analysis to study the effects of Reynolds number on flow characteristics of vehicle. Three different velocities (10 m/s, 20 m/s and 30 m/s) were considered and it was found that 2–5% drag reduction could be achieved for different configurations and Reynolds numbers.

As the conditions of the Mars environment and Earth environment are appreciably different e.g. the environment of Mars is characterized by very low density and a lower viscosity than that of the Earth [36], to have efficient vehicles on Mars, every aspect of vehicles especially their aerodynamics must be well understood.

This research work discusses the aerodynamic study of the wake region of Ahmed body in both Martian environment and Earth environment. The results obtained for Mars environment are compared from those obtained for Earth environment. The aerodynamic study is conducted with the help of computational fluid dynamics (CFD). To the best of authors 'knowledge, no similar work is conducted so far despite its paramount importance.

II. Methodology

2.1 Geometry Selection

The Ahmed body is selected for the aerodynamic analysis in both Martian and Earth environment as represented in Figure 1. The Ahmed body was first proposed and studied by Ahmed et al.,[37]. It is a fundamental car geometry containing a uniform front with bowed edges and an acute slant angle at the top of the rear. The slant angle φ possesses an effective impact on the outcomes of drag as well as lift. Ahmed et al., showed that the slant angle is an effective and a key parameter for analyzingdrag and lift coefficient for Ahmed body[38]. TheAhmed body used in this analysis has standard dimensions which are identical to the work performed by Ahmed et al.,[38]. The flow features are obtained and studied for different rear slant angles of the Ahmed body as the change in slant angle significantly influence the flow characteristics. The three slant angles used in this study are φ=25°, φ=30° and φ=35°. The selected slant angles are frequently explored by different researchers in the previous research to analyze the wake flow characteristics[33, 39-44].Figure 1 indicates all the dimensions used for Ahmed body in this research work. The origin point is indicated where X, Y and Z coordinates are zero (0, 0, 0). The axes directions are also shown in Figure 1. The origin points and axis directions both are made standard and will remain same throughout this research work. In first case, the slant angle is taken as -25° with respect to positive X- axis. In second case, the slant angle is taken as -30° with respect to positive X- axis and in the third case; the slant angle is taken as -35° with respect to positive X- axis. The first case, second case and third case will be referred in this research work as 25° slant angle case, 30°slant anglecase and 35°slant anglecase respectively.

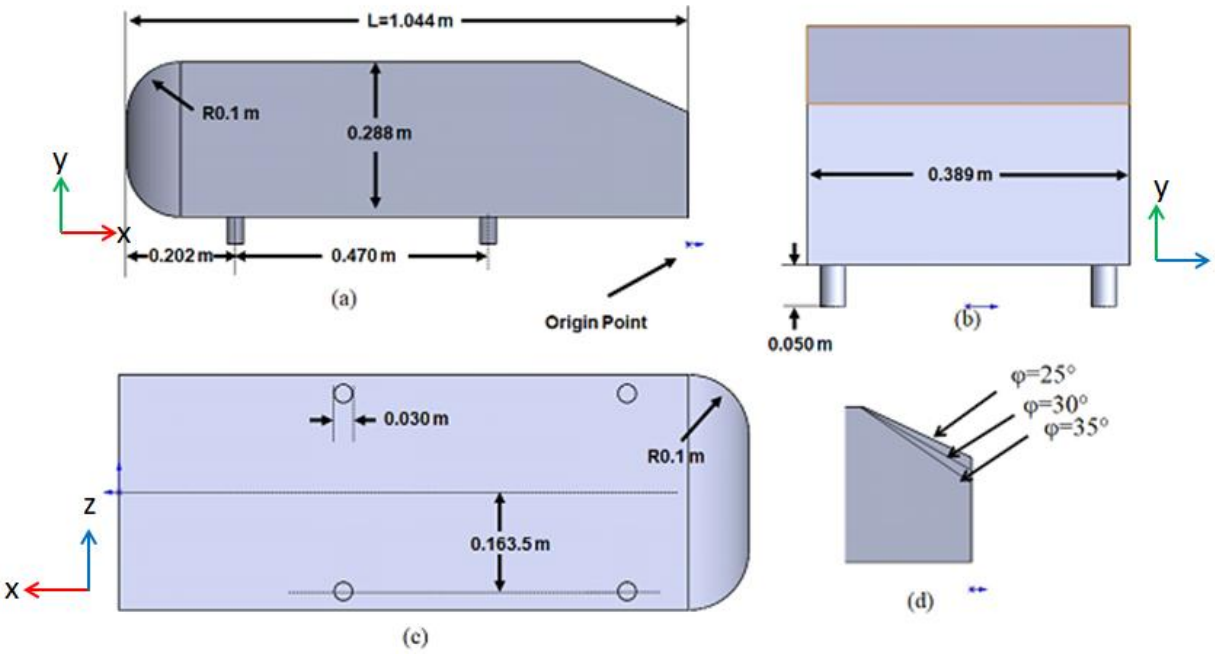

Figure 1: (a) Ahmed body with dimension and origin axes (b) Front side of Ahmed body (c) Bottom side of Ahmed body (d) Rear side of Ahmed body with different slant angles.

2.2 Computational Domain

The computational domain for numerical simulation is shown in Figure 2.The walls of computational domain are selected far apart i.e., 2.5L from the front of Ahmed body, 5L from the back of Ahmed body, 2L above theAhmed body and 2L from each side of Ahmed body; where L is the total length of Ahmed body. This will ensure that the walls of computational domain have no effect on the flow characteristics around Ahmed body[45, 46]. The blockage ratio for this computational domain is approximately equal to one. The blockage ratio minimization has a positive effect on computational fluid dynamics results obtained from virtual wind tunnel analyses[47-49]. The symmetry plane is shown in Figure 2which divides the computational domain and Ahmed body into two symmetrical halves. The half symmetry plane saves the computational time and cost as number of elements arereduced to half without compromising the computational accuracy and it is a commonly applied technique[50].

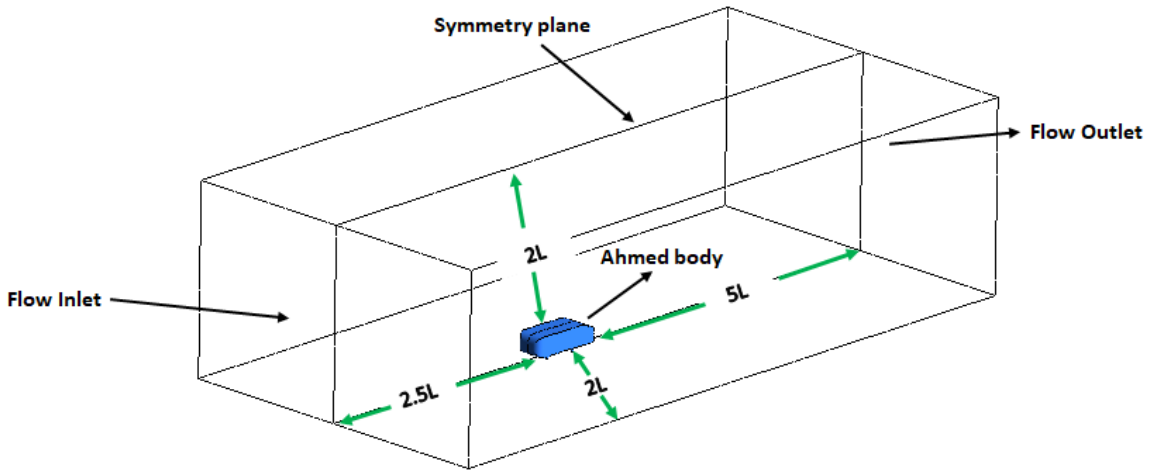

Figure 2: Computational domain for numerical simulation

2.3 Meshing

In ANSYS meshing module, hybrid meshing approach is used to perform meshing of the computational domain. In order to generate the mesh, automatic meshing algorithm approach is used[51]. Different refinement zones are created to control the mesh with dense mesh zones on critical portions of domain [52, 53]. In order to reduce the computational error; a growth rate of 1.2 (20%) is applied to each zone with the intentions that adjacent cells raise steadily, based on comprehensive literature survey[46, 50, 54]. Inflation layer with prismatic elements is developed on Ahmed body and road surface to have better results near shear walls, which is a commonly reported technique[55-57].There is a good alignment of the elements in the prismatic layer with the flow near wall boundary, and this kind of mesh near the walls also causes reduction in the numerical diffusion[58]. Tetrahedral elements are used for entire domain with controlled growth rate [59, 60].The widespread use of tetrahedral cells in computational analysis is owed to them being more efficient compared to the other meshing element types and also due to the reason that the tetrahedral mesh generation techniques generate high definition mesh [61].The selected meshed computational domain is shown in Figure 3.

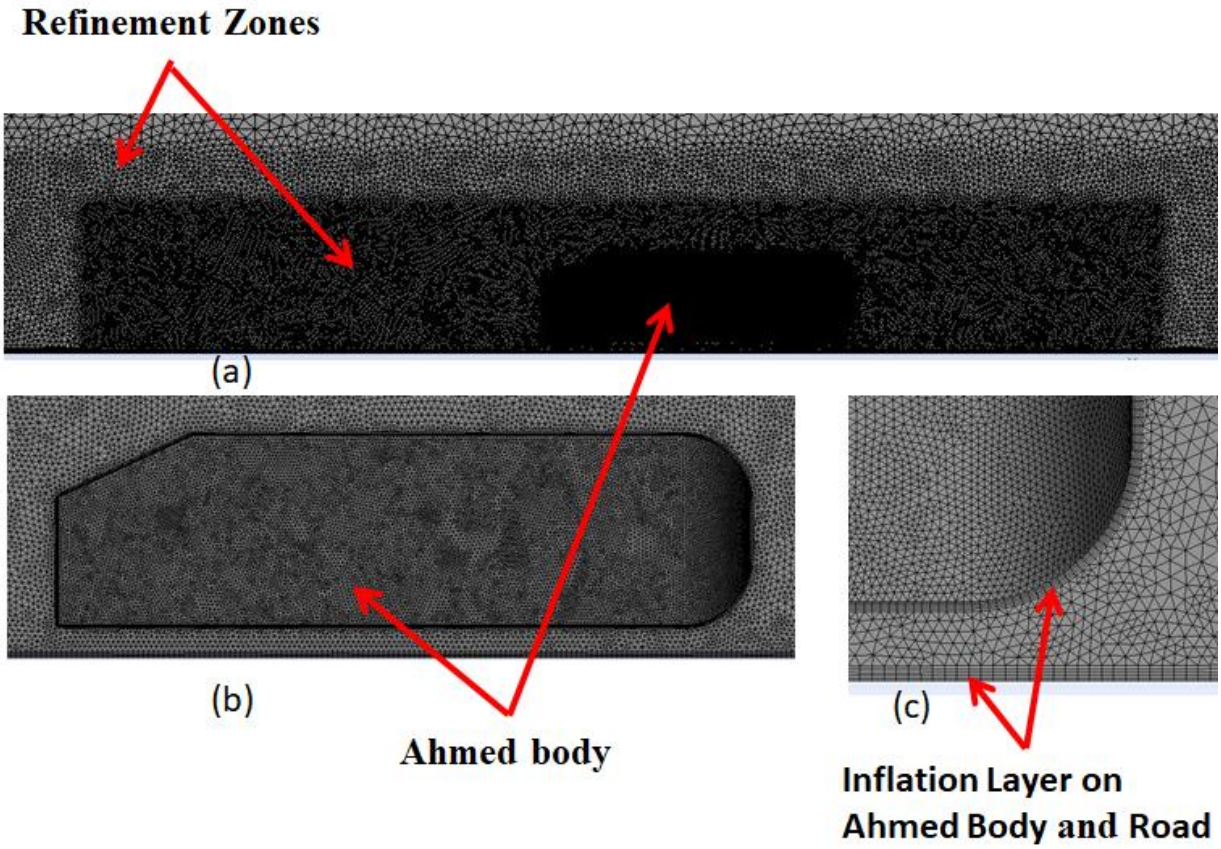

Figure 3: (a) Refinement zones in computational domain (b) Meshed Ahmed body (c) Inflation layer on Ahmed body and road.

A comprehensive mesh independence study is conducted to find the mesh configuration for which the mesh does not considerably affect the result.The number of elements in the computational domain is systematically increased by bringing down the size of cellsand the corresponding percentage relative difference in coefficient of drag and coefficient of lift is observed. The percentage relative error for coefficient of drag and coefficient of lift gradually decrease with the increase in number of cells. The reduction in the cell size is continued until the percentage relative error of less than 2% is achieved[54, 62]. The mesh independence analysis is shown in Figure 4, percentage relative error is observed on ordinate and number of elements are observed on abscissa along with a horizontal line showing 2% relative error[63].The mesh independence analysis is conducted up to 2×10^7 elements and the last seven different element configurations do not give a percentage relative error above 2%. Further, increasing the number of elements can cause increasingly high computational cost compared to negligible reduction in relative error. Computational domain with 1.8×10^7 elements is selected as a final domain for CFD analysis after performing mesh independence analysis.

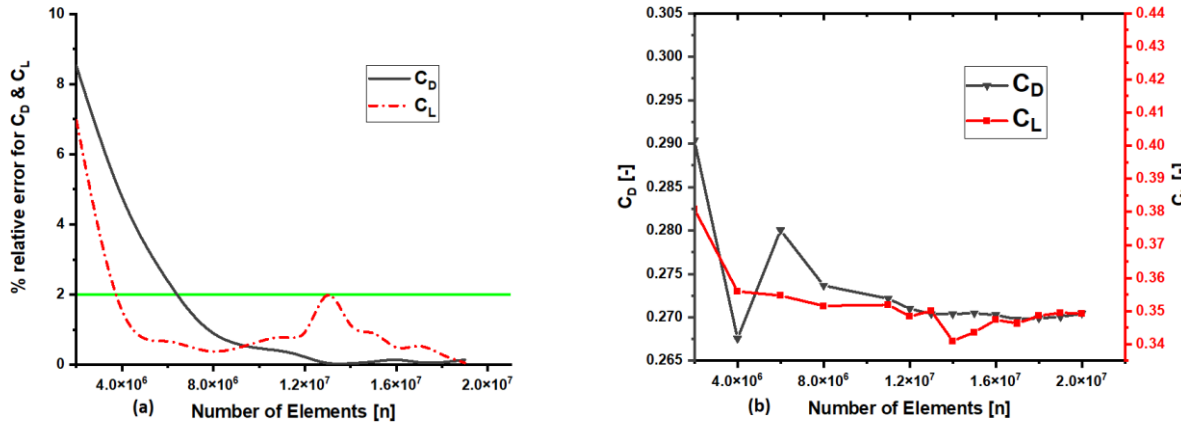

Figure 4: (a) Percentage relative error for coefficient of drag and lift with increasing number of elements (b) Coefficient of drag and lift with increasing mesh resolution

2.4 Numerical Model Configuration

In this research, LES based analyses are performed for computer simulated experimentation. A hybrid RANS-LES approach is used to analyze the wake flow characteristics ofAhmed body[28, 64-66].The selection between the models such as RANS or LES is reliant on the resources of computer system and the level of accuracy required in the flow simulation. RANS model is commonly adopted when the computation is performed in the industries. Although RANS model are effective in predicting various parts of the flow nearby an automobile, they have been reported to be incompetent to predict the unsteadiness in the wake areas[67, 68].A hybrid RANS-LES performs better as compared to other models such as Spalart Allmaras, Realizable k – ε, k − ω SST etc.[69].The value of Reynold number used to standardize the computer simulation experimentation is 2.78×10^6[25, 70]. No-slip wall condition is applied on each wall of the computational domain and the road is considered as stationary[71, 72]. The blockage ratio (ratio of the frontal area of Ahmed body to the frontal area of computational domain) calculated in this study is approximately equal to one[42, 73].The minimization of blockage ratio gives better results for computer simulated experimentation.The Sub-Grid Scales (SGSs) stress tensor model adopted for this study was Dynamic Smagorinsky-Lily model (DSM)[67, 74]. The DSM model is the modified form of Smagorinsky-Lily model (SM). The major difference between the function of these two models is the value of Smagorinsky model constant, C_s[75]. A constant value of C_s is used in case of SM but in case of DSM, value for Cs is dynamically calculatedthrough the LES [74].The coupled pressure-velocity scheme was adopted along with second-order upwind discretization for momentum, second-order upwind discretization for pressure, and second-order implicit transient formulation. A time-step size of 5×10^{-5} second is used for the simulation setup.The two equation realizable K-Ɛ model is used to obtain the initial flow characteristics in the computational domain[76].The LES model is then used to obtain flow behavior around the Ahmed body for different velocities and slant angles.The terminationcriteria are set so that the solution reach a convergence point where the continuity residual reaches 10^{-5} and velocity residual reaches 10^{-9}.

Navier-Stokes equations and continuity equations are the fundamental equations in the fluid flow problems. The governing LES equations (1 and 2 mentioned below) used in this study are derived from above said fundamental equations.

$$\frac{\partial \bar{u}_j}{\partial x_j} = 0 \qquad (1)$$

$$\frac{\partial \bar{u}_i}{\partial t} + \frac{\partial \bar{u}_j\,\bar{u}_i}{\partial x_j} = -\frac{1}{\rho}\frac{\partial \bar{p}}{\partial x_i} + \frac{\partial}{\partial x_j}\left(\nu \frac{\partial\ \bar{u}_i}{\partial x_i}\right) + \frac{1}{\rho}\frac{\partial \tau_{ij}}{\partial x_j} \qquad (2)$$

Here, ν = kinematic viscosity

$\bar{u}_i$ = filtered variables for the resolved velocity

$\bar{p}$ = filtered variables for the resolved pressure

τ_{ij} = SGS turbulent stress , which is defined in equation 3:

$$\tau_{ij} = \overline{u_i u_j} - \bar{u}_i \bar{u}_j \qquad (3)$$

The DSM model is modified form of Smagorinsky-Lily model (SM). The major difference between the function of these two models is the value of Smagorinsky model constant, C_s [75]. A constant value of C_s is used in case of SM but in case of DSM, value for C_s is dynamically calculated through the LES [74]. In order to create separation between smaller scales and resolve field, DSM model makes use of a test filter,$\tilde{\Delta}$. This test filter is double in size of the size of grid filter, Δ [75] and is used in Navier-Stokes equations which results in another quantity called subtest-scale stress defined as

$$T_{ij} = \widetilde{u_i u_j} - \tilde{u}_i \tilde{u}_j \quad (4)$$

Where symbol "□" represents the test-filtered variables. It can be seen that SGS turbulent stress τ_{ij} and subtest-scale stress T_{ij} are related through dynamic Smagorinsky constant as mentioned in equation 5.

$$T_{ij} - \tilde{\tau}_{ij} = L_{ij} \quad (5)$$

Using dynamic Smagorinsky constant, another factor known as dynamic Smagorinsky model constant, C_{ds}, is defined as given in equation 6.

$$C_{ds} = \left(\frac{L_{ij} M_{ij}}{M_{ij} M_{ij}} \right)^{\frac{1}{2}} \quad (6)$$

Where M_{ij} in equation 6 is defined in equation 7

$$M_{ij} = -2 \left(\tilde{\Delta}^2 |\widetilde{\bar{S}}| \widetilde{\bar{S}_{ij}} - \bar{\Delta}^2 |\widetilde{\bar{S}}| \widetilde{\bar{S}_{ij}} \right) \quad (7)$$

2.5 Boundary Conditions

The Ahmed body is considered stationaryand fluid is considered to flow around it. This configuration is similar to the actual wind tunnel test configuration[25]. The fluid is flowing in positive X-direction as shown in Figure 5.

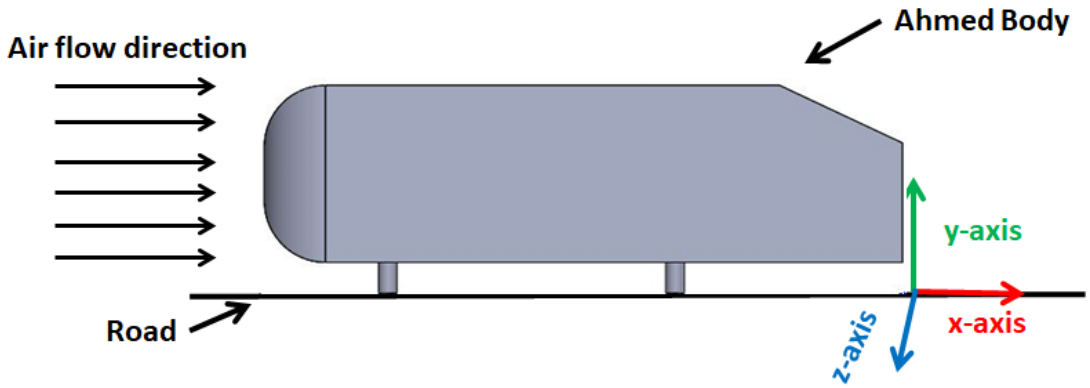

Figure 5: Direction of flow Stream

The properties used for both Mars case and Earth case in this study are summarized in Table 1.Average temperature and atmospheric density for both Mars and Earth case is taken from the previous research work[77, 78]. Atmospheric pressure in Martian environment is obtained from NASA LaRC model and JPL data[79].Average gravitational acceleration on Mars is taken as 3.71 ms^{-2}[78, 80-82].The value of air viscosity for both Mars and Earth case is used from the previous research work[80].

Table 1: Properties used in simulation

Properties	Mars Case	Earth Case	Units
Density	0.0138	1.225	$kg\text{-}m^{-3}$
Atmospheric pressure	790	101325	$N\text{-}m^{-2}$
Viscosity	0.000013	0.0000178	$kg\text{-}m^{-1}\text{-}s^{-1}$
Gravitational acceleration	3.71	9.81	$m\text{-}s^{-2}$
Average Temperature	210.16	288.16	K

2.6 Computer Simulated Experimental Configuration

In this research, the computer simulated experimentation is performed at different slant angles in order to study the wake profile of Ahmed body as the flow characteristics aresignificantly altered by considering

different rear slant angles. The rear slant angles used in this study are φ=25°, φ=30° and φ=35°[83, 84].Three different velocity configurations i.e., 18.6 ms^{-1}, 24.2 $ms^{-1}$and 30.6 $ms^{-1}$are selected to study the flow characteristics of Ahmed body wake in Mars environment in comparison with Earth environment[46, 85]. The computer simulated experimentation is verified with experimental results available in previous studies[25, 38, 64].The velocity used for verification process is 40 ms^{-1}. Average temperature (288.16K for Earth case and 210.16K for Mars case) is used to study the flow characteristics of Ahmed body for both Mars and Earth case [77, 78]. The temperature with the value of 298.16K is used for true comparison on both Mars and Earth case [86].Experimental configuration is summarized in Table 2.

Table 2: Variable used in Simulation

Variables	Values
Slant Angle	25°, 30°, 35°
Velocity (m/s)	18.6, 24.2, 30.6
Temperature (K)	288.16, 298.16 for Earth case, 210.16, 298.16 for Mars case

III. Results and Discussion

In this research, aerodynamic analysis of Ahmed body for Earth and Mars environment is studied using CFD. The results for the computer simulated experimentation are obtained by applying hybrid RANS-LES model. The comparative results for both Earth and Mars case which includes coefficient of drag, coefficient of lift, velocity profile, Q-criterion and velocity contour are discussed in thissection. The functional definition of coefficient of lift and coefficient of drag is as follows:

Drag Coefficient:

Drag coefficient is a particular number that describes the dependency of drag force on complex parameters i.e., flow characteristic, object shape and flow conditions etc., the drag coefficient is represented by C_D.

Lift Coefficient:

Lift coefficient is a particular number that describes the dependency of lift force on complex parameters i.e., flow characteristic, object shape and flow conditions etc., the lift coefficient is represented by C_L.

3.1 Comparison of Numerical Simulation and Experimental Results

Ahmed, S.R., et al. and Lienhart et al., conducted the experimental study to analyse the flow charactristics of Ahmed body. The comparion of numerical study in the present case and the experimetal results are discussed in 3.1.1 and 3.1.2. These sections clearly indicates that the simulation results in present study are in close agrement with the experimental results published previously.

3.1.1 Comparison of C_D& C_L for Current Simulation Based Analysis and Experimental Analysis

The simulation results are compared with the experimental results to find out the validity of model used in present study[25, 33]. The Reynold number and slant angle used for both simulation and experimental configuration are2.78×10^6 and 25° respectively.Simulation results are in close agreement with wind tunnel experimental study of Ahmed bodyin Earth environment. The validity of computer simulated model is represented inFigure 6.

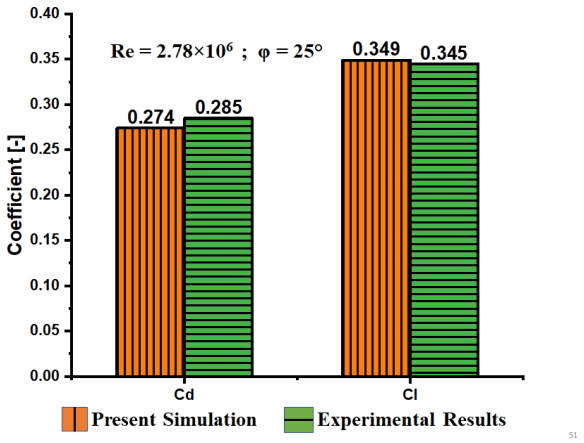

Figure 6: The C_D&$C_L$for presentsimulation based analysis and experimental analysis[25, 33]

3.1.2 Comparison between Experimental Results vs Present Study for Velocity Profile

The velocity profile for x-velocity component corresponding to different locations in wake region is compared with the experimental results. The X and Y distances are made as non-dimension entity by dividing them with the length L of Ahmed body. The x velocity component is divided by the far field velocity U□. The *Y/L* is shown on ordinate and *u/U*□ is represented on abscissaThe experimental and numerical results are compared in Figure 7. The boundry conditions set for numerical model are identical to the the experimental configuration [87].Lienhart et al.,had conducted an inclusive experimental study of the flow charactristics emerging around the Ahmed body. The experiment was performed in a ¾ open test-section[87]. Flow charactrictics of Ahmed body with 25° slant angle and inlet velocity of 40ms^{-1} were studied in the experimentation. The numerical flow profiles closely agrees with the experimetal flow profies as shown in Figure 7.

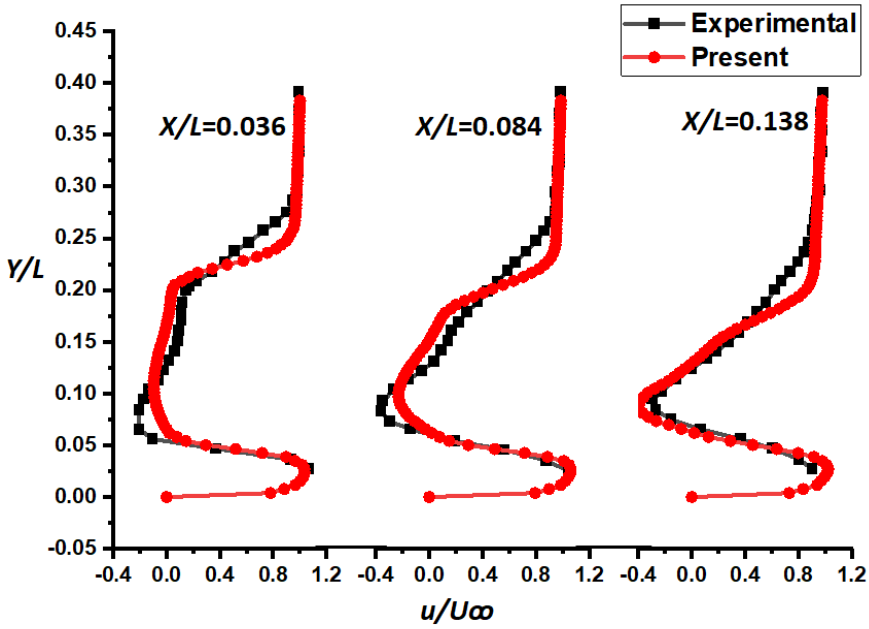

Figure 7: Comparison between experimental results vs present study for velocity profile for the x-velocity component at different wake region distances for 40 m/s velocity

3.2 Coefficient of Drag vs Velocity

The coefficient of dragof Ahmed bodyfor Earth and Mars environmentis shown inFigure 8. Results are evaluated for three different velocities i.e., 18.6 ms^{-1}, 24.2 ms^{-1}and 30.6ms^{-1}.InFigure 8(a),the coefficient of dragand velocity with the slant angle φ=25° are shown on ordinate and abscissa respectively.Whereas, the legend E288 represents earth case at 288.16K temperature, M210 represents Mars case at 210.16K temperature, E298 represents earth case at 298.16K temperature and M298 represents Mars case at 298.16K temperature.The decreasing trend of C_D with respect to increase in velocity for both Earth case and Mars case is observed. A higher coefficient of drag is observed for the Martian environment corresponding tothe Earth's environment for the same Ahmed body. As the velocity is increased from 18.6 m/s to 24.2 m/s then the slope of C_D stated the drag reduction of 4.16% for Earth case and 4.78% for Mars case. Similarly, when the velocity is increased from 24.2 m/s to 30.6 m/s then, the drag reduction of 3.6% and 5.02% is observed for Earth case and Mars case respectively. The similar behavior can be observed for the slant angles φ=30° and φ=35° as shown in the Figure 8(b) and Figure 8(c) respectively. If the true comparison is taken at same temperature (T=298.16K) for both Earth case and Mars case then C_D value for Mars case is generally lesser as compared to Earth as shown in theFigure 8.

The decrease in coefficient of drag with the increase in velocity can be explained by studying the wake region of Ahmed body.A negative or vacuum pressure exists at the closest wake region of Ahmed body when it is subjected to fluid flow. This vacuum pressure region in wake keeps pulling the vehicle opposite to its movement in fluid. The difference between coefficient of drag values for both cases decrease as velocity increases. There exists approximately 2.5 times coefficient of drag for Mars case at 18.6 meter per second velocity corresponding to Earth case, but this difference keeps on decreasing and at 30.6 meter per second velocity, the coefficient of drag for Mars case become 2.43 times of Earth case. The trend lines for both cases

suggest that as the velocity increase the difference in $C_D$decreases.The c-pillar vortex is also important to study as they play a vital role in flow detachment[88].A highly detach flow can have a negative impact on wake flow characteristics;therefore, the flow detachment should be controlled and made beneficial by design improvements. By studying aerodynamic profile of flow field around Ahmedbody, a new design approach can be made for vehicles designed for Mars specifically for low velocity vehicles.

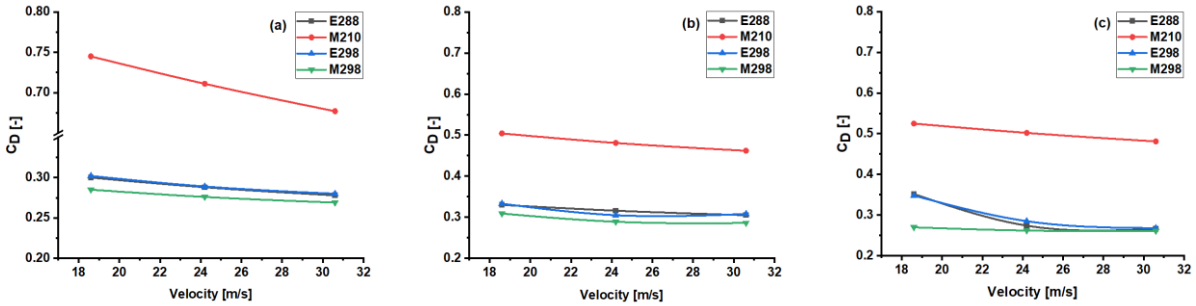

Figure 8: (a) Coefficient of drag of Ahmed body with slant angle φ=25° (b) Coefficient of drag of Ahmed body with slant angle φ=30° (c) Coefficient of drag of Ahmed body with slant angle φ=35°

The comparison between Earth and Mars cases in Figure 8 partially signifies the gravitational effect as other factors are also effecting the final results. The effect of gravity is usually being neglected in literature however, a pure gravity based analysis is required for a practically accurate design. The effect of density on coefficient of drag can be analyzed by comparing the coefficient of drag at different temperatures. The percentage increment or decrement in coefficient of drag with respect to temperature differenceΔT is presented in Figure 9 (a). A higher density effect can be observed in Mars cases comparative to the Earth cases. The comparative analysis is made on the basis of percentage change in coefficient of drag for each degree temperature change.This normalization gives us a true picture for both environments and it can be observed that the density effect is more critical in Martian environment.Specifically, for slant angle φ=25° this effect is maximum. The Figure 9 (b) and Figure 9 (c) indicates coefficient of pressure for both temperature values i.e., 210K and 298K, slant angle φ=25°, and velocity 30.6 m/s. From A-pillar to C-pillar region negative Cp indicates the highly turbulent nature of flowing fluid for 210K case and comparison between both 210K case and 298K case clearly represents the dominant negative Cp region for 210K case. Moreover, a larger negative C_p region at the start of slant and in the wake region for 210K confirms higher C_D for lower densities. The flow mass is deficient in the above mentionedregions (start of slant and the wake region for 210K case) creating negative pressure zones with larger vortices and vacuum drag.

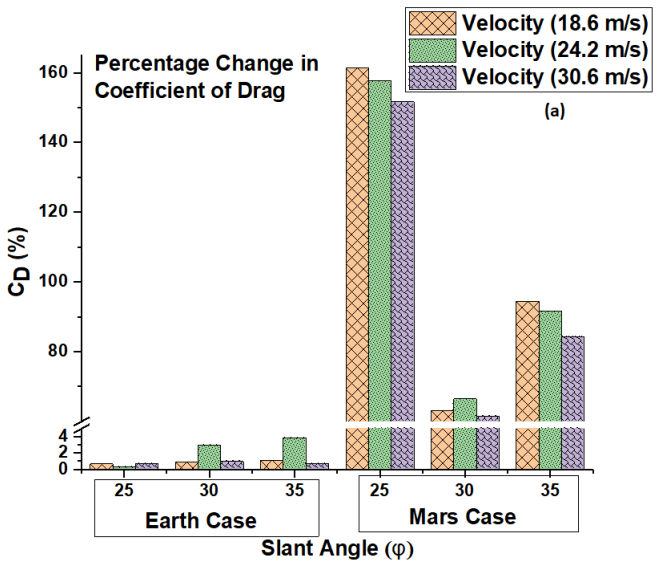

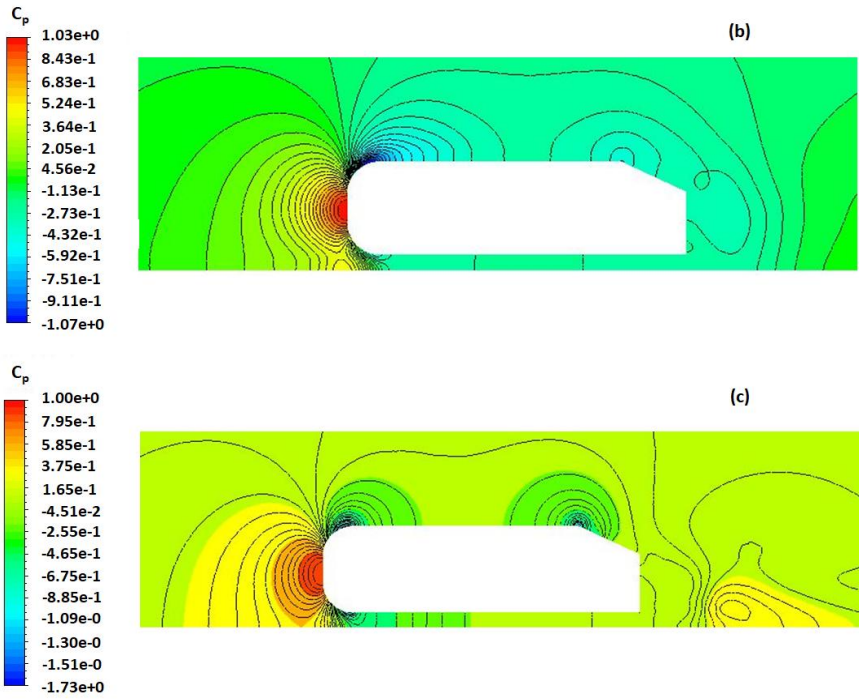

Figure 9: (a) Percentage change in coefficient of drag forΔT with different operating conditions (b) Coefficient of pressure for slant angle φ=25°, velocity 30.6 m/s and 210K temperature(c) Coefficient of pressure for slant angle φ=25°, velocity 30.6 m/s and 298.16K temperature

3.3 Coefficient of Lift Vs Velocity

The coefficient of lift of Ahmed body for both Mars and Earth environment is shown inFigure 10. InFigure 10, the velocity and the slant angle of φ=25° is represented on abscissa and ordinate respectively. It is observed fromFigure 10(a) that the value of $C_L$decreases with the increase in velocity,this behavior is similar as that of drag case. As the velocity is increased from 18.6 m/s to 24.2 m/s, the lift reduction of 3.54% for Mars case and 1.94% for Earth case is noticed. Similarly, when the velocity is increased from 24.2 m/s to 30.6 m/s, the lift reduction of and 8.21% and 2.27% is observed for Mars case and Earth case respectively.Figure 10(b) and the Figure 10(c) indicates the similar behavior for the value of C_L for the slant angle of φ=30° and φ=35° respectively. If the true comparison is taken at same temperature (T=298.16K) for both Mars case and Earth case then C_L value for Mars case is lower as compared to Earth for the slant angle of φ=25° and φ=30°as shown in the Figure 10(a) and Figure 10(b).For the slant angle φ=35°, there is a maximum reduction in the value of $C_L$for Earth case with the increase in velocity when it is compared with other two slant angles (φ=25° and φ=30°)as shown in the Figure 10(c).This result is consistent with the previous work of Ahmed et. al., and Drage et. al., [33, 73].

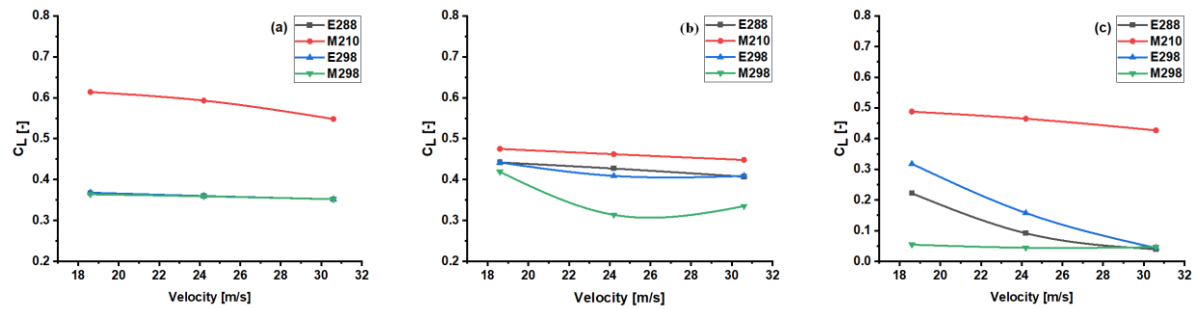

Figure 10: (a) Coefficient of lift of Ahmed body with slant angle φ=25° (b) Coefficient of lift of Ahmed body with slant angle φ=30° (c) Coefficient of lift of Ahmed body with slant angle φ=35°

The change in coefficient of lift for different operating conditions can be also attributed to gravity and atmospheric density.Thin Martian atmosphere requires lower CL for vehicle stability.A higher

increment/decrement can be observed in Mars cases comparative to the Earth cases with the unit temperature change. The percentage increment or decrement in coefficient of lift with respect to temperature difference ΔT is represented in Figure 11 (a). Both in Earth and Mars environment maximum change in CL is obtained for slant angle φ=35°. The Figure 11 (b) and Figure 11 (c) indicates velocity streamlines (Mars case) for both temperature values i.e., 210K and 298K, slant angle φ= 35° and velocity 24.2 m/s. The higher flowing fluid velocity over Ahmed body will reduce the pressure above it creating higher lift values for 210K case Figure 11 (b). Comparatively higher velocity zones are observed at A-pillar and C-pillar regions for 210K case aiding in higher coefficient of lift.

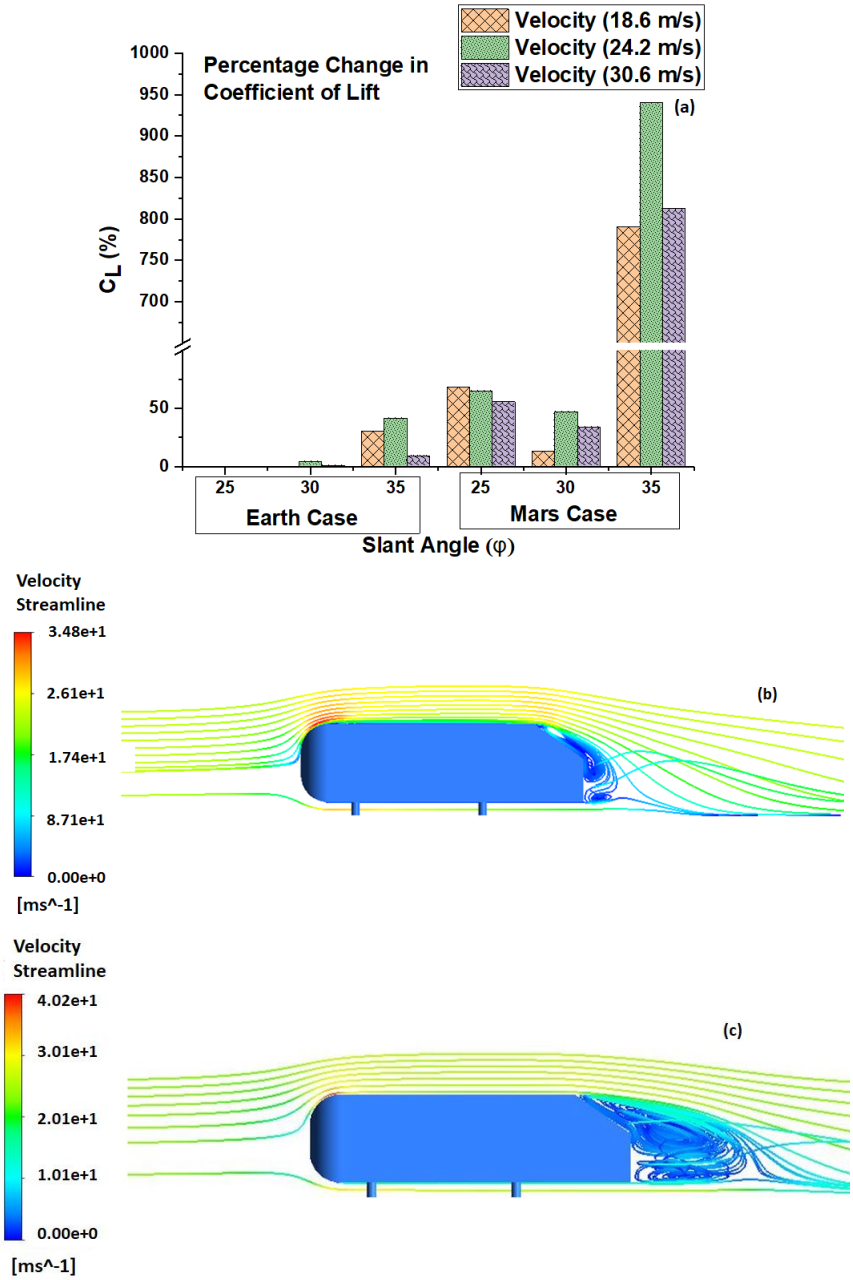

Figure 11: Percentage change in coefficient of lift for ΔT with different operating conditions (b) Stream lines for slant angle φ=35°, velocity 24.2 m/s and 210K temperature (c) Stream lines for slant angle φ=35°, velocity 24.2 m/s and 298.16K temperature

3.4 Velocity Profile for the X-Velocity Component at Different Wake Region Distances

The velocity profile for the x-velocity component at different wake region is shown inFigure 12toFigure 14. The X and Y distances are made as non-dimension entity by dividing them with the length L of Ahmed body. The x velocity component is divided by the far field velocity U□. The *Y/L* is shown on ordinate

and *u/U*□ is represented on abscissa. The values of *u/U*□ aretaken at a point where*X/L* is equal to 0.036, 0.138 and 0.228. The Z is kept constant at zero to approach thevalues of x velocity at symmetry plane.Four cases are discussed in each diagramto represent the different scenarios for Mars and Earth. The details of mentioned cases are Earth case at 288.16K temperature represented by E288, Mars case at 210.16K temperature represented by M210, Earth case at 298.16K temperature represented byE298 and Mars case at 298.16K temperature represented by M298.

3.4.1 The velocity Profile at 18.6 m/s Velocity

The velocity profile for Mars case and Earth case can be used to understand the difference in flow characteristics in both environments. The understanding and comparative study of flow features can help in design decision process.The velocity profile for Mars case and Earth case with the velocity of 18.6 m/s at three different slant angles (φ=25°, φ=30° and φ=35°) is shown in theFigure 12.The velocity profile with the slant angle of 25° is shown in Figure 12(a). At *X/L* equal to 0.036, velocity profile mismatch for Mars case for almost entire velocity profile as compared to Earth caseat average temperature except for the region where*Y/L*0.18-0.11. Experimental configuration (density, viscosity and temperature) used in the Martian environment has lower values than that of Earth which results in a working condition having lower Reynolds number.Therefore, the flow characteristics in Martian environment are appreciably different fromthat of Earth environment[36]. For Mars case at average temperature, the velocity ratio is less than 1 forall the values of*Y/L* which indicates the start of negative wake region. From *Y/L* 0.27-0.00 the velocity ratio is negative indicating vortex region where the particles started to swirl[41, 64]and this phenomena increase the coefficient of drag.For Earth case at average temperature, the velocity ratio is less than 1 at *Y/L* equal to 0.28 which indicates the start of negative wake region. From *Y/L* 0.19-0.07 the velocity ratio is negative indicating vortex region where the particles started to swirl.Whereas, the fluid flow coming from the underbody compensate the wake region upto velocity ratio of 1.Mars and Earth case at the temperature 298K shows approximately similar behavior.

The velocity ratio relatively remains a greater portion in between 0.8-1with the increase of *X/L* for Earth case due to the diminishing effect of generated vortex caused by flow detachments [41, 64].In the same *X/L* advancement region the Mars case shows that the negative wake region is still growing having an adverse effect on the flow features.

The velocity profile with the slant angle of 30° is shown in Figure 12(b). At *X/L* equal to 0.036,for Mars case at average temperature, the velocity ratio is less than 1 at *Y/L*0.37 which indicates the start of negative wake region. From *Y/L* 0.17-0.06 the velocity ratio is negative which is smaller than 25° slant angle case. Whereas, the fluid flow coming from the underbody compensate the wake region up to velocity ratio of 0.7. Mars and Earth case at the temperature 298K shows approximately same behavior expect for the region from *Y/L* 0.24-0.11.

The velocity ratio with the progression of *X/L* displays a similar behavior as observed for 25° slant angle for Earth case. However, for Mars case, the velocity ratio relatively remains a larger portion in between 0.8-1 with the increase of *X/L*when compared with the 25° slant angle case andwith the progression of *X/L*, the regain of velocity ratio is comparatively greater than 25° slant angle case. The 30° slant angle case performs better in terms of flow characteristics in Martian environment as compared with 25° slant angle case.

The velocity profile with the slant angle of 35° is shown in Figure 12(c). At *X/L* equal to 0.036, for Mars case at average temperature, the velocity profile shows approximately same behavior as observed for 30° slant angle.For Mars case at 298K temperature, it is observed that the flow detachment start early in 35° slant angle case and retains its effect longer than the previous studied slant angles.For Earth case at average temperature, the velocity ratio is less than 1 at *Y/L* equal to 0.30 which indicates the start of negative wake region. From *Y/L* 0.25-0.06 the velocity ratio is negative which is smaller than 25° slant angle case but larger than 30° slant angle case.

For Earth case at average temperature, the flow detachment starts early in 35° slant angle case when compared with previous studied slant angles i.e., 25° and 30°. It was observed that for 18.6 m/s velocity, the best performance in terms of flow characteristics for Mars case can be obtained for 30° slant angle irrespective of temperature change.

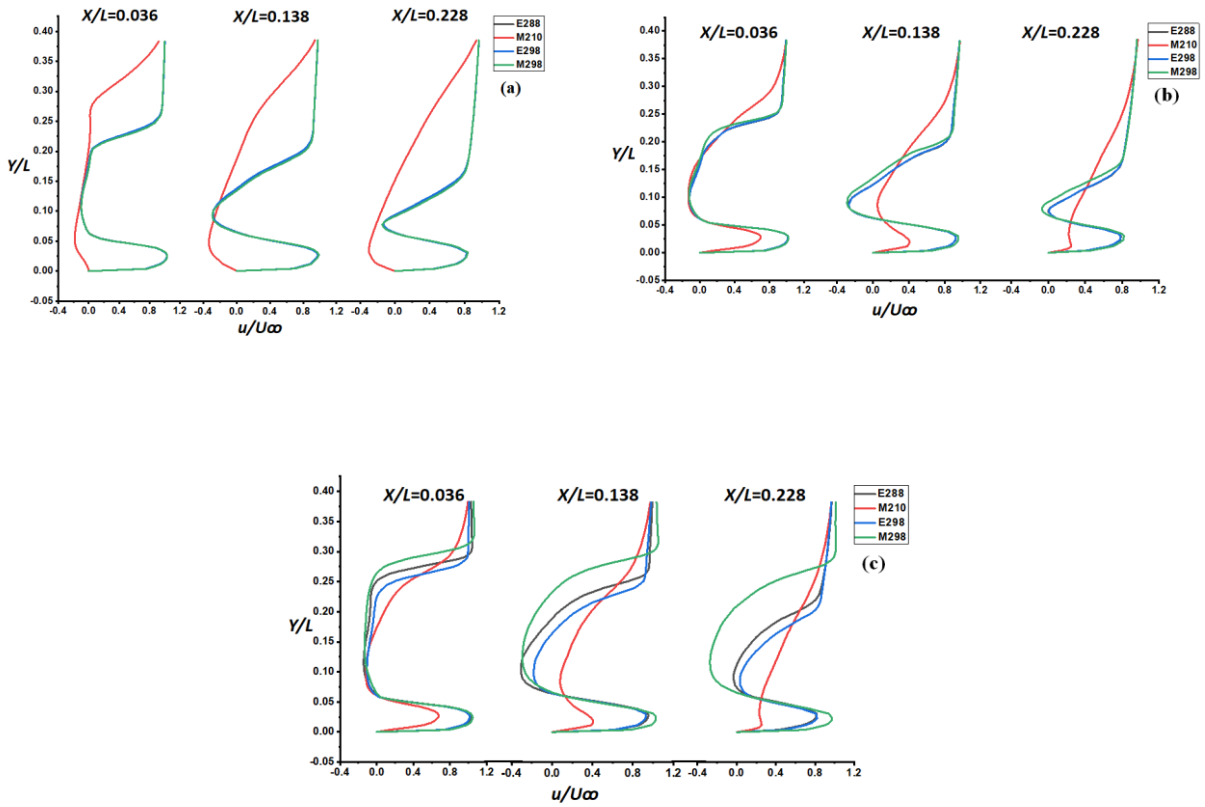

Figure 12: Velocity profile for the x-velocity component at different wake region distances for 18.6 m/s velocity for different slant angle cases (a) φ=25° (b) φ=30° (c) φ=35°

3.4.2 The Velocity Profile at 24.2 m/s Velocity

The velocity profile for Mars case and Earth case with the velocity of 24.2 m/s at three slant angles (φ=25°, φ=30° and φ=35°) is shown in theFigure 13. The velocity profile with the slant angle of 25° is shown in Figure 13(a).For Mars case at *X/L* equal to 0.036,almost the entire velocity profile mismatch except for the region between *Y/L* 0.2-0.1.For Mars case at average temperature, the velocity profile shows approximately similar behavior observed for the 18.6 m/s velocity. Similarly, the Mars and Earth case at the temperature 298K shows approximately same behavior as observed in the previous case for 18.6 m/s.

The velocity ratio remains more in between 0.8-1 for Earth case with the *X/L*increment; this is due to the diminishing effect of generated vortex caused by flow detachments same as observed for 18.6 m/s velocity[41, 64]. In the same region, the Mars case show that the negative wake region is still growing having an adverse effect on the flow characteristics.

The velocity profiles with the slant angles of 30° and 35° are shown in Figure 13(b) and Figure 13(c). At *X/L* equal to 0.036, for Mars case at average temperature and for 30° and 35° slant angles,the velocity profile shows approximately similar behavior observed for the 18.6 ms^{-1} velocitybecause the density and viscosity used in the Martian environment has much lower values than those at Earth resulting in a minor change in Reynold number with the increase in velocity[36].Therefore, change in velocity has negligible effect on the velocity profile. Mars and Earth case at the temperature 298K shows approximately same behavior except for the region*Y/L* 0.38-0.12which is greater as compared to 18.6m/s velocity case.

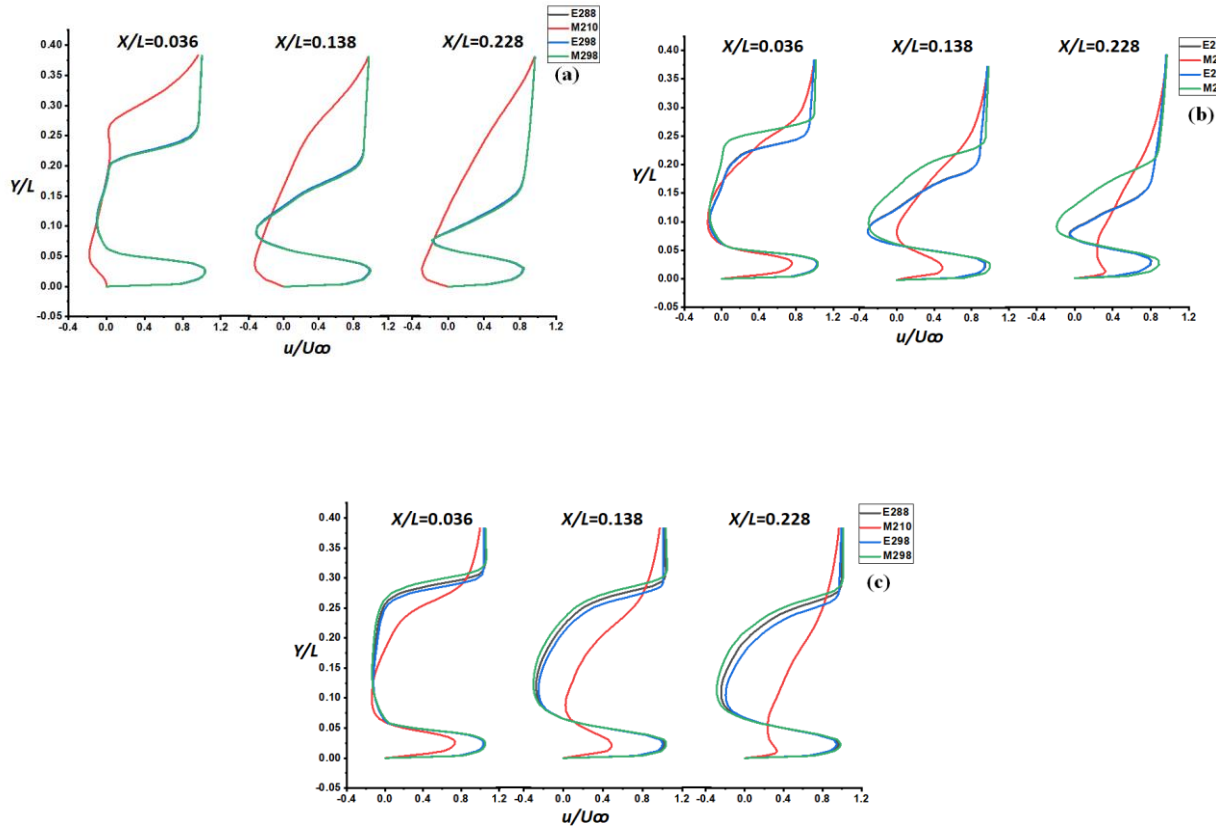

Figure 13: Velocity profile for the x-velocity component at different wake region distances for 24.2 m/s velocity for different slant angle cases (a) φ=25° (b) φ=30° (c) φ=35°

3.4.3 The Velocity Profile at 30.6 m/s Velocity

The velocity profile for Mars case and Earth case with the velocity of 30.6 m/s at three slant angles (φ=25°, φ=30° and φ=35°) is shown in theFigure 14. The velocity profile with the slant angle of 25° is shown in Figure 14(a). At *X/L* equal to 0.036, velocity profile mismatch for Mars case for almost whole velocity profile except for the region between *Y/L* 0.2-0.17.For Mars case at average temperature, the velocity profile shows approximately similar behavior observed for the 24.2 m/s velocity except the negative velocity ratio region which is from *Y/L* 0.18-0.03. This negative velocity ratio region is less as compared to the velocity ratio region observed in cases of 18.6 m/s and 24.2 m/s velocity.Therefore, the coefficient of drag in 30.6 m/s velocity case is lower as compared to the previous velocity cases.

The velocity profile with the slant angle of 30° and 35° are shown in Figure 14(b) and Figure 14(c). At *X/L* 0.036-0.228, for Mars case at average temperature, the velocity profile indicates a higher flow detachment and vortex generation corresponding to the 30° and 35° slant angle case of 24.2m/s.

The resistance to flow detachment is prolonged (for 298K temperature) with the increase of velocity for all the angles of Mars and Earth case except 30° Mars case and 35° Earth case where a negligible assistance to flow detachment is observed.

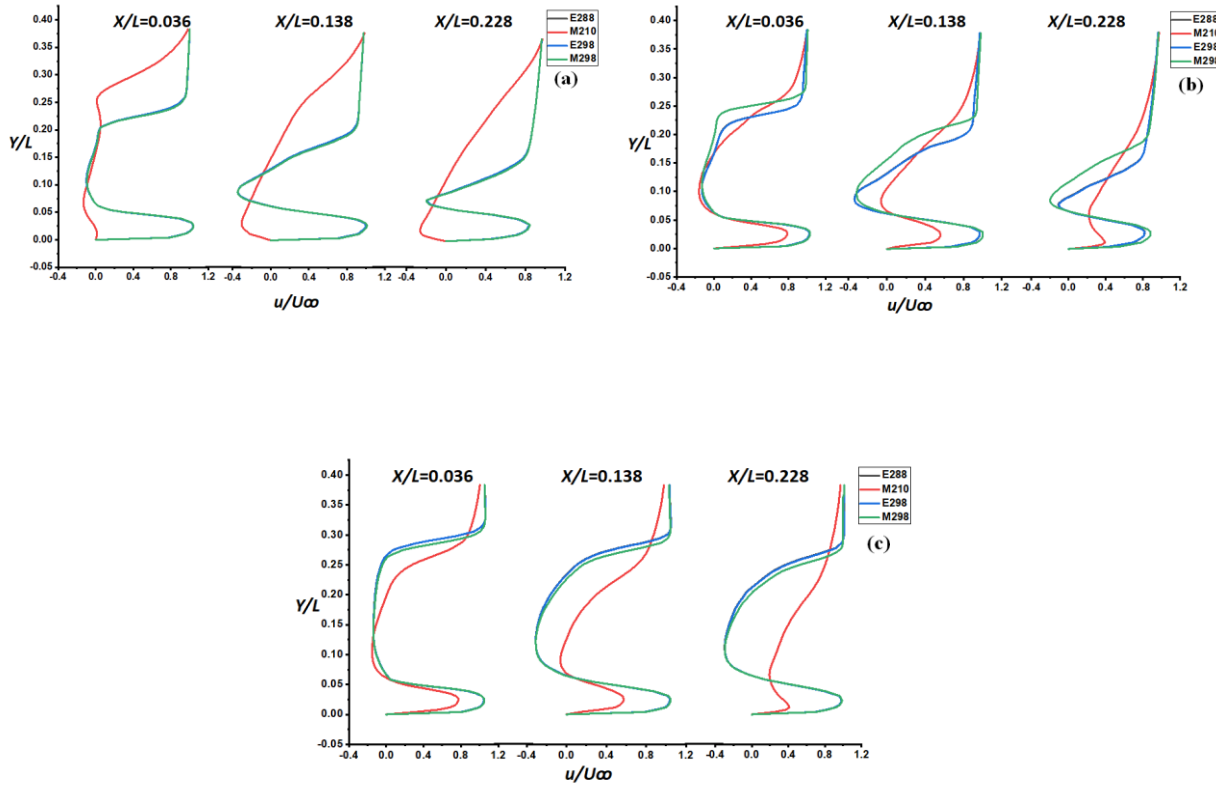

Figure 14: Velocity profile for the x-velocity component at different wake region distances for 30.6 m/s velocity for different slant angle cases (a) φ=25° (b) φ=30° (c) φ=35°

The comparison between Figure 12-Figure 14confirms that as the slant angle of Ahmed body is changed from 25° to 35°, the fluid flow profile for Mars case become more and more identical to Earth case.It is concluded that the Ahmed body with 30° slant angle gives best performance for Mars caseat average temperature with the increase in velocity. At 298K temperature, it is observed that 35° slant angle for both Mars and Earth case with the increase in velocity gives best performance[39].

3.5 Flow Structure Using Q-criterion

The vortices formation, flow structure and intensity of flow rotation can be identified by using classical Q-criterion method. This method is used to analyze turbulent nature of flow and helps in identifying critical vertical structures e.g., hairpins, flow detachments, separation bubbles and vortex tubes etc.The Q-criterion presented here is used to analyze fore and rear Ahmed body flow structure. Figure 15 represent the selected cases of Martian environment for the analysis of flow structure. The selected cases has following specifications; Figure 15 (a & b): slant angle φ=25°, velocity 30.6 m/s and 298.16K temperature, top and isometric view respectively, Figure 15 (c & d): slant angle φ=25°; velocity 30.6 m/s and 210K temperature, top and isometric view respectively. Lower first and second vortex can be seen in both cases. The intensity of first lower vortex is high for 298.16K temperature case compared to 210K case however, the vortex rotational flow area is small Figure 15 (a & c). This leads to higher turbulent flow in the lower stream for 210K case. A small second lower vortex can be identified foe 298.16K case and a very large second lower vortex can be identified for 210K case that indicates the influence of first lower vortex in underbody region creating a highly turbulent structureFigure 15 (b & d). The fore body nose separation bubbles are formed due to the high vorticity in both cases. These separation bubbles will trail downstream towards backlight region and influence the rear region for 210K case. Similar behavior can be observed for fore body side region in both cases. A high vortex region is observed at the start of slant for both cases however, for 298.16K case the reattachment of flow is obtained very early compared to 210K case. This results is also in line with the discussion in section 3.2. C-Pillar vortices for 210K case has also have higher influence in turbulent wake region creating higher drag values. Overall, higher vortex formation can be observed for 210K case that leads to higher coefficient of drag.

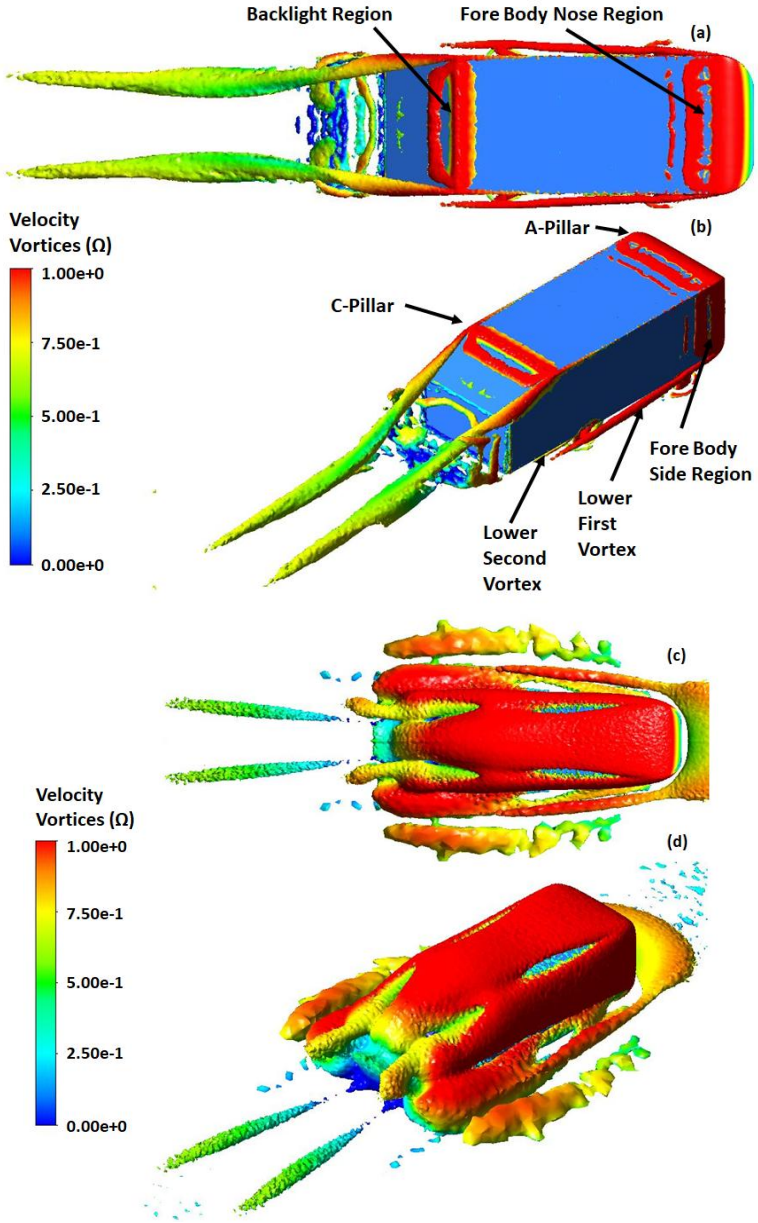

Figure 15: Q-criterion showing velocity vortices (a) Mars case, slant angle φ=25°, velocity 30.6 m/s and 298.16K temperature, top view (b) Mars case; slant angle φ=25°, velocity 30.6 m/s and 298.16K temperature, isometric view(c) Mars case, slant angle φ=25°; velocity 30.6 m/s and 210K temperature, top view (d) Mars case; slant angle φ=25°, velocity 30.6 m/s and 210K temperature, isometric view

3.6 Velocity Contours in Y-Z Plane

The non-dimensional velocity contour in Y-Z plane at *X/L* equals to 0 and 0.48 for 30.6 m/s velocity and for both cases at average temperatureis shown inFigure 16. The non-dimensional velocity value is obtained by dividing velocity on each point of computational domain with far field velocity U□.Velocity contours are plotted with the case of 30° slant angle of Ahmed body.Adistinguishable c-pillar vortex is obtained for 30° slant angle at 30.6 m/s velocity for both Mars and Earth case. At *X/L* equals to zero, the c-pillar vortex generated in Mars case is larger than Earth case and a heavy region of recirculation is formed.At *X/L* equals to 0.48, the recirculation is vanished however a huge velocity deficit in the core is observed in both Mars and Earth case. The velocity deficit in Mars case is greater as compared to Earth case. It can be perceived from Figure 16that the pressure recovery in Earth case is faster than Mars case and the pressure drop is high in Mars case as compared to Earth case.Therefore, the coefficient of drag at average temperature is higher in Mars case as compared to the Earth case.

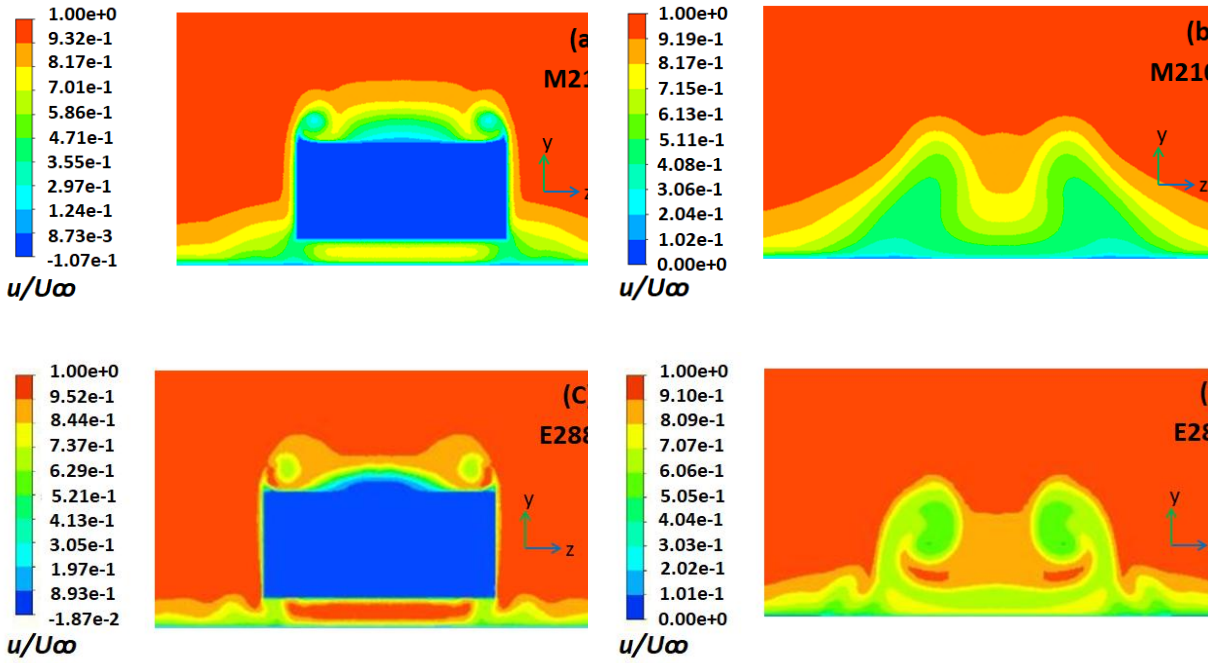

Figure 16: Velocity contours in Y-Z plane with 30° slant angle for Mars case (a-b) and Earth case (c-d) at *X/L* = 0 (a and c) and *X/L* = 0.48 (b and d)

The non-dimensional velocity contour in Y-Z plane at *X/L* equals to 0 and 0.48 for 30.6 m/s velocity and for both cases at 298K temperature is shown inFigure 17.Velocity contours are plotted with the case of 35° slant angle of Ahmed body. This is the true comparison between Mars and Earth case for the flow characteristics of Ahmed body at same temperature (298K).At *X/L* equals to zero, the c-pillar vortex generated in Earth case is larger than Mars case and a comparatively larger region of recirculation is appeared. At *X/L* equals to 0.48, the recirculation is vanished however a huge velocity deficit in the core is observed in both Mars and Earth case. The velocity deficit in Earth case is greater as compared to Mars case. It can be perceived fromFigure 17that the pressure recovery in Mars case is faster than Earth case and the pressure drop is high in Earth case as compared to Mars case. Therefore, the coefficient of drag at same temperature (298K) is higher in Earth case as compared to the Mars case.

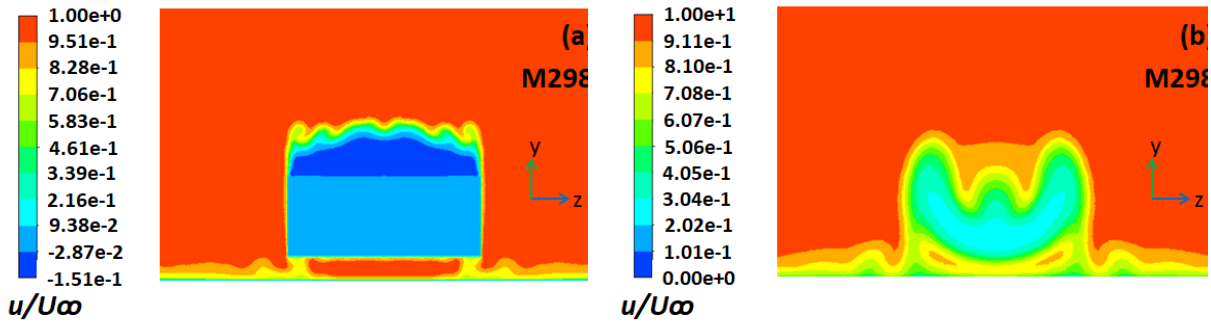

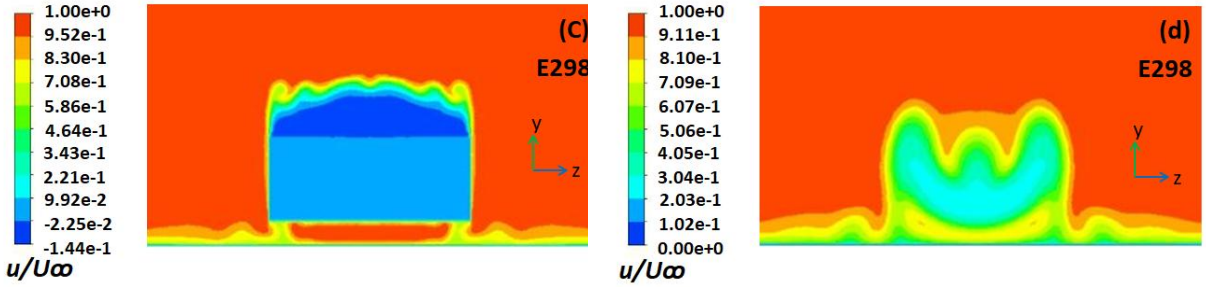

Figure 17:Velocity contours in Y-Z plane with 35° slant angle for M
ars case (a-b) and Earth case (c-d) at *X/L* = 0 (a and c) and *X/L* = 0.48 (b and d)

In previous research work, it is observed that the varying temperature is only responsible of negligible coefficient of drag variation in Earth environment[46]. In this study, a noticeable difference in coefficient of drag is observed by varying the temperature for Mars environment. Mars environment have different zones with different temperatures ranges. Therefore, it is necessary to develop the C-pillar profile in such a way that it could be changed with the change in temperature in Mars environment.

IV. Conclusion

The aerodynamic study of wake region of Ahmed body on Martian environment, as compared to Earth environment was performed and it is the first attempt to understand the flow characteristics around the Ahmed body in Martian environment. The hybrid RANS-LES model was applied to perform computer simulation at different slant angles (φ=25°, φ=30° and φ=35°) with three different velocity configurations i.e., 18.6 ms^{-1}, 24.2 ms^{-1} and 30.6 ms^{-1}. Average temperatures of 210.16K and 288.16K were used to study the flow characteristics of Ahmed body on Mars and Earth respectively. The temperature of 298.16K was used for the true comparison for both Martian and Earth environment. Following important points have been concluded from this study:

1) Comparison of $C_D$values obtained from current simulation with those obtained from experimentation performed at Earth at 40 ms^{-1} and25° slant angle showed that there is a close agreement between the two
2) Similarly, velocity profiles obtained from simulation were compared with the corresponding profiles obtained from experimentation. The comparison showed that both profiles closely match
3) The coefficient of drag (C_D) was higher in Martian environment than that of the Earth's environment for the same Ahmed body at average temperature. Moreover, $C_D$was found to decrease with the increase in velocity for both cases
4) The C_D of Ahmed body at Mars was approximately 2.5 times the coefficient of drag at Earth corresponding to the velocity i.e., 18.6 ms^{-1}, but this factor kept on decreasing with the increase in velocity e.g., its value was about 2.43 times (instead of 2.5 times) corresponding to 30.6 ms^{-1} velocity at 25° slant angle and at average temperature
5) The true comparison was made at same temperature (T=298.16K) for bothMars and Earth case which indicated that C_D for Mars case is less than that of the Earth case
6) The velocity profile observed at selected points of wake region for both Mars and Earth case at average temperatures indicated that there was a total mismatch between the velocity profiles. This may be due to the working condition characterized by lower Reynolds number for Mars case; therefore, the flow characteristics in Martian environment are different from the Earth
7) The velocity profile, as explained above, was observed at same temperature (298.16K) which showed approximately similar behavior for both Mars and Earth with 25° slant angle, however, the behavior was different in case of 30° and 35° slant angles
8) It was also found that the Ahmed body with 30° slant angle gives the best performance for Mars case at average temperature with the increase in velocity. However, at the temperature of 298K, which was used for true comparison between the Mars and Earth case, it was observed that 35° slant angle gives the best performance
9) In this study, a noticeable difference in coefficient of drag was observed by changing the temperature for Mars environment. Mars environment have different zones with different temperatures ranges. Therefore, it is necessary to develop the C-pillar profile in such a way that it could be changed with the change in temperature in Martian environment

References:

[1]. Davila, A.F. and D.J.A. Schulze-Makuch, The last possible outposts for life on Mars. 2016. **16**(2): p. 159-168.
[2]. Mahaney, W.C. and J.J.J.o.C. Dohm, Life on Mars? Microbes in Mars-like antarctic environments. 2010. **5**: p. 951-958.
[3]. Edwards, H.G., et al., Raman spectroscopic analysis of cyanobacterial colonization of hydromagnesite, a putative martian extremophile. 2005. **175**(2): p. 372-381.
[4]. Cockell, C.S. and J.A.J.I. Raven, Zones of photosynthetic potential on Mars and the early Earth. 2004. **169**(2): p. 300-310.
[5]. de Vera, J.-P., et al., Adaptation of an Antarctic lichen to Martian niche conditions can occur within 34 days. 2014. **98**: p. 182-190.
[6]. Niles, P., et al., Scientific Investigations Associated with the Human Exploration of Mars in the Next 35 Years. 2017.
[7]. Hoffman, S., Human Mars Mission Overview and Dust Storm Impacts on Site Selection. 2017.
[8]. Rucker, M.A., Human Mars Surface Mission Nuclear Power Considerations. 2018.
[9]. Rucker, M., Dust Storm Impacts on Human Mars Mission Equipment and Operations. 2017.
[10]. Levchenko, I., et al., Mars colonization: beyond getting there. 2019. **3**(1): p. 1800062.
[11]. Sun, Y., et al., A numerical study of fluid flow and heat transfer in carbon dioxide enclosures on mars. 2018. **11**(4): p. 756.
[12]. Seol, M.-L., et al., Triboelectric nanogenerator for Mars environment. 2017. **39**: p. 238-244.
[13]. Rucker, M.A., et al., Solar Versus Fission Surface Power for Mars. 2016.
[14]. Harris, K.E., et al., Mass Optimization of a Supercritical CO2 Brayton Cycle Power Conversion System for a Mars Surface Fission Power Reactor. 2017. **3**(3): p. 031006.
[15]. Park, J.H., et al., Transient analysis and validation with experimental data of supercritical CO2 integral experiment loop by using MARS. 2018. **147**: p. 1030-1043.
[16]. Sheller, M., Automotive Emotions:Feeling the Car. 2004. **21**(4-5): p. 221-242.
[17]. Polsgrove, T., et al. Mars ascent vehicle design for human exploration. in AIAA SPACE 2015 Conference and Exposition. 2015.
[18]. Kleinhenz, J.E. and A. Paz. An ISRU propellant production system for a fully fueled Mars Ascent Vehicle. in 10th Symposium on Space Resource Utilization. 2017.
[19]. Prince, A., et al., Mars Ascent Vehicle (MAV) Solid Motor Technology Plans. 2019.
[20]. Merrill, R.G., et al. An Integrated Hybrid Transportation Architecture for Human Mars Expeditions. in AIAA SPACE 2015 Conference and Exposition. 2015.
[21]. Tai, W.S., D.S. Abraham, and K.-M. Cheung. Mars Planetary Network for Human Exploration Era–Potential Challenges and Solutions. in 2018 SpaceOps Conference. 2018.
[22]. Green, R.D. and J.E. Kleinhenz, In-Situ Resource Utilization (ISRU) Living off the Land on the Moon and Mars. 2019.
[23]. Beaty, D., et al., Some strategic considerations related to the potential use of water resource deposits on Mars by future human explorers. 2016.
[24]. Huminic, A. and G.J.I.J.o.A.T. Huminic, Aerodynamic study of a generic car model with wheels and underbody diffuser. 2017. **18**(3): p. 397-404.
[25]. Meile, W., et al., Experiments and numerical simulations on the aerodynamics of the Ahmed body. 2011. **3**(1): p. 32-39.
[26]. Mohammadikalakoo, B., et al., Passive flow control on Ahmed body by rear linking tunnels. 2020. **205**: p. 104330.
[27]. Bayraktar, I., D. Landman, and O.J.S.t. Baysal, Experimental and computational investigation of Ahmed body for ground vehicle aerodynamics. 2001: p. 321-331.
[28]. Guilmineau, E., et al. Assessment of RANS and DES methods for the Ahmed body. in ECCOMAS Congress 2016-VII European Congress on Computational Methods in Applied Sciences and Engineering. 2016.
[29]. Guilmineau, E., et al., Assessment of hybrid RANS-LES formulations for flow simulation around the Ahmed body. 2018. **176**: p. 302-319.
[30]. Spalart, P.R. Comments on the feasibility of LES for wings, and on a hybrid RANS/LES approach. in Proceedings of first AFOSR international conference on DNS/LES. 1997. Greyden Press.
[31]. Ashton, N., et al., Assessment of RANS and DES methods for realistic automotive models. 2016. **128**: p. 1-15.
[32]. Tunay, T., et al., Effects of rear slant angles on the flow characteristics of Ahmed body. 2014. **57**: p. 165-176.
[33]. Ahmed, S.R., G. Ramm, and G.J.S.T. Faltin, Some salient features of the time-averaged ground vehicle wake. 1984: p. 473-503.
[34]. Meile, W., et al., Non-symmetric bi-stable flow around the Ahmed body. 2016. **57**: p. 34-47.
[35]. Bello-Millán, F., et al., Experimental study on Ahmed's body drag coefficient for different yaw angles. 2016. **157**: p. 140-144.
[36]. Mauricio J. García, R.D.H.E.M.R.M.A.A., Analysis of an Aerodynamic Profile to Generate Sustaination in the Mars Atmosphere. International Journal of Advanced Science and Technology, 2020. **29**(05): p. 14054 - 14069.
[37]. Ahmed, S.R., G. Ramm, and G. Faltin, Some salient features of the time-averaged ground vehicle wake. 1984, SAE Technical Paper.
[38]. Ahmed, S.R., G. Ramm, and G. Faltin, Some Salient Features of the Time -Averaged Ground Vehicle Wake. SAE Transactions, 1984. **93**: p. 473-503.
[39]. Mohammadikalakoo, B., P. Schito, and M. Mani, Passive flow control on Ahmed body by rear linking tunnels. Journal of Wind Engineering and Industrial Aerodynamics, 2020. **205**: p. 104330.
[40]. Morel, T., The Effect of Base Slant on the Flow Pattern and Drag of Three-Dimensional Bodies with Blunt Ends, in Aerodynamic Drag Mechanisms of Bluff Bodies and Road Vehicles, G. Sovran, T. Morel, and W.T. Mason, Editors. 1978, Springer US: Boston, MA. p. 191-226.
[41]. Tunay, T., B. Sahin, and V. Ozbolat, Effects of rear slant angles on the flow characteristics of Ahmed body. Experimental Thermal and Fluid Science, 2014. **57**: p. 165-176.
[42]. Joseph, P., X. Amandolese, and J.-L.J.E.i.f. Aider, Drag reduction on the 25 slant angle Ahmed reference body using pulsed jets. 2012. **52**(5): p. 1169-1185.
[43]. Strachan, R., K. Knowles, and N.J.E.i.f. Lawson, The vortex structure behind an Ahmed reference model in the presence of a moving ground plane. 2007. **42**(5): p. 659-669.
[44]. Wang, X., et al., Turbulent near wake of an Ahmed vehicle model. 2013. **54**(4): p. 1-19.
[45]. Keogh, J., et al., The aerodynamic effects on a cornering Ahmed body. 2016. **154**: p. 34-46.
[46]. Uddin, G.M., et al., Artificial intelligence-based Monte-Carlo numerical simulation of aerodynamics of tire grooves using computational fluid dynamics. 2019. **33**(3): p. 302-316.
[47]. Das, P., et al., Large eddy simulation of the flow-field around a full-scale heavy-duty truck. 2013. **56**: p. 521-530.
[48]. Blocken, B., Y.J.J.o.W.E. Toparlar, and I. Aerodynamics, A following car influences cyclist drag: CFD simulations and wind tunnel measurements. 2015. **145**: p. 178-186.
[49]. Collin, C., T. Indinger, and J.J.I.J.o.A.E. Müller, Moving ground simulation for high performance race cars in an automotive wind tunnel. 2017. **8**(1): p. 15-21.

[50]. Uddin, G.M., et al., Neural networks assisted computational aero-acoustic analysis of an isolated tire. 2020. **234**(10-11): p. 2561-2577.
[51]. Haag, L., T. Blacha, and T.J.I.J.o.A.E. Indinger, Experimental investigation on the aerodynamics of isolated rotating wheels and evaluation of wheel rotation models using unsteady CFD. 2017. **8**(1): p. 7-14.
[52]. Abohela, I., N. Hamza, and S.J.R.E. Dudek, Effect of roof shape, wind direction, building height and urban configuration on the energy yield and positioning of roof mounted wind turbines. 2013. **50**: p. 1106-1118.
[53]. Strumolo, G.S. and V. Babu, Method and system for providing a virtual wind tunnel. 2000, Google Patents.
[54]. Ahmad, N.E., E. Abo-Serie, and A.J.C.L. Gaylard, Mesh optimization for ground vehicle aerodynamics. 2010. **2**(1): p. 54-65.
[55]. Grabowski, L., et al. Application of CAD/CAE class systems to aerodynamic analysis of electric race cars. in IOP Conference Series: Materials Science and Engineering. 2015. IOP Publishing.
[56]. Holder, J.M., B. Malla, and E.J. Gutmark. CFD Analysis on Single Expansion Ramp Nozzle Performance. in 2018 AIAA Aerospace Sciences Meeting. 2018.
[57]. Wang, S., et al., The effect of the ground condition on high-speed train slipstream. 2018. **172**: p. 230-243.
[58]. Lanfrit, M., Best practice guidelines for handling Automotive External Aerodynamics with FLUENT. 2005, Version.
[59]. Wong, K.H., et al., 3D CFD simulation and parametric study of a flat plate deflector for vertical axis wind turbine. 2018. **129**: p. 32-55.
[60]. Kallinderis, Y.J.I.j.f.n.m.i.f., Adaptive hybrid prismatic/tetrahedral grids. 1995. **20**(8-9): p. 1023-1037.
[61]. Yamakawa, S. and K. Shimada, Fully-automated hex-dominant mesh generation with directionality control via packing rectangular solid cells. 2003. **57**(15): p. 2099-2129.
[62]. Diasinos, S., T.J. Barber, and G. Doig, The effects of simplifications on isolated wheel aerodynamics. Journal of Wind Engineering and Industrial Aerodynamics, 2015. **146**: p. 90-101.
[63]. Ahmad, N.E., E.F. Abo-Serie, and A.J.C.L. Gaylard, Mesh optimization for ground vehicle aerodynamics. 2010. **2**(1): p. 54-65.
[64]. Guilmineau, E., et al., Assessment of hybrid RANS-LES formulations for flow simulation around the Ahmed body. Computers & Fluids, 2018. **176**: p. 302-319.
[65]. Keogh, J., et al., The aerodynamic effects on a cornering Ahmed body. Journal of Wind Engineering and Industrial Aerodynamics, 2016. **154**: p. 34-46.
[66]. Inagaki, M., T. Kondoh, and Y.J.J.F.E. Nagano, A mixed-time-scale SGS model with fixed model-parameters for practical LES. 2005. **127**(1): p. 1-13.
[67]. Inagaki, M., T. Kondoh, and Y. Nagano, A mixed-time-scale SGS model with fixed model-parameters for practical LES, in Engineering Turbulence Modelling and Experiments 5. 2002, Elsevier. p. 257-266.
[68]. Guilmineau, E., et al. Assessment of hybrid LES formulations for flow simulation around the ahmed body. in Turbulence and Interactions. 2015. Springer.
[69]. Ashton, N., et al., Assessment of RANS and DES methods for realistic automotive models. Computers & Fluids, 2016. **128**: p. 1-15.
[70]. Rao, A., et al., On the two flow states in the wake of a hatchback Ahmed body. Journal of Wind Engineering and Industrial Aerodynamics, 2018. **173**: p. 262-278.
[71]. Serre, E., et al., On simulating the turbulent flow around the Ahmed body: A French–German collaborative evaluation of LES and DES. Computers & Fluids, 2013. **78**: p. 10-23.
[72]. Krajnović, S. and L. Davidson, Flow around a simplified car, part 1: large eddy simulation. 2005.
[73]. Gabriel, A., et al. Efficient use of computational fluid dynamics for the aerodynamic development process in the automotive industry. in 26th AIAA Applied Aerodynamics Conference. 2008.
[74]. Ekman, P., et al., Importance of Sub-Grid Scale Modeling for Accurate Aerodynamic Simulations. 2021. **143**(1): p. 011501.
[75]. Germano, M., et al., A dynamic subgrid-scale eddy viscosity model. 1991. **3**(7): p. 1760-1765.
[76]. Shih, T.-H., et al., A new k-ϵ eddy viscosity model for high reynolds number turbulent flows. 1995. **24**(3): p. 227-238.
[77]. Bézard, H., et al. Aerodynamic design of a Martian micro air vehicle. in ODAS 2019. 2019.
[78]. Collins, N.S., System Design and Nonlinear State-Dependent Riccati Equation Control of an Autonomous Y-4 Tilt-Rotor Aerobot for Martian Exploration. 2016: University of Surrey (United Kingdom).
[79]. Colozza, A., Solid State Aircraft. NASA Inst. for Advanced Concepts, Atlanta, GA, Final Report, Phase II Project, NAS5-03110, 2005.
[80]. Almeida, M.P., et al., Giant saltation on Mars. 2008. **105**(17): p. 6222-6226.
[81]. Gelhar, S.R. Designing Mars Missions for the Utilization of Rotorcraft. in Proceedings of the Wisconsin Space Conference. 2019.
[82]. Koning, W.J., W. Johnson, and H.F.J.A.J. Grip, Improved Mars helicopter aerodynamic rotor model for comprehensive analyses. 2019. **57**(9): p. 3969-3979.
[83]. Guilmineau, E., Effects of Rear Slant Angles on the Flow Characteristics of the Ahmed Body by IDDES Simulations. 2018, SAE Technical Paper.
[84]. Liu, K., et al., Flow structure around a low-drag Ahmed body. Journal of Fluid Mechanics, 2021. **913**: p. A21.
[85]. Leśniewicz, P., M. Kulak, and M. Karczewski. Vehicle wheel drag coefficient in relation to travelling velocity-CFD analysis. in Journal of Physics: Conference Series. 2016. IOP Publishing.
[86]. Catalfamo, C., et al., High temperature Mars atmosphere. Part II: transport properties. 2009. **54**(3): p. 613-621.
[87]. Lienhart, H. and S. Becker, Flow and Turbulence Structure In the Wake of a Simplified Car Model. SAE Transactions, 2003. **112**: p. 785-796.
[88]. Corallo, M., J. Sheridan, and M.C. Thompson, Effect of aspect ratio on the near-wake flow structure of an Ahmed body. Journal of Wind Engineering and Industrial Aerodynamics, 2015. **147**: p. 95-103.